Shape optimization of a layer by layer mechanical constraint for additive manufacturing

Grégoire Allaire, Charles Dapogny, Alexis Faure, Georgios Michailidis

SHAPE OPTIMIZATION OF A LAYER BY LAYER MECHANICAL CONSTRAINT FOR ADDITIVE MANUFACTURING

G. ALLAIRE[1], C. DAPOGNY[2], A. FAURE [3], AND G. MICHAILIDIS [3]

[1] *CMAP, École polytechnique, CNRS UMR 7641, 91128 Palaiseau, France*,
[2] *Laboratoire Jean Kuntzmann, CNRS, Université Grenoble-Alpes, BP 53, 38041 Grenoble Cedex 9, France*,
[3] *SIMaP, Université Grenoble-Alpes, BP 53, 38041 Grenoble Cedex 9, France.*

Abstract. The purpose of this note is to introduce a new functional of the domain, to be used in shape optimization problems as a means to enforce the constructibility of shapes by additive manufacturing processes. This functional aggregates the self-weights of all the intermediate structures of the shape appearing in the course of its layer by layer assembly. Its mathematical analysis is outlined and an algorithm is proposed to accelerate the significant computational effort entailed by the implementation of these ideas. Eventually, a numerical validation and a concrete example are discussed.

Résumé. Nous introduisons dans cette note une nouvelle fonctionnelle dépendant du domaine qui, utilisée comme contrainte dans un problème d'optimisation de forme, impose la constructibilité par les procédés de fabrication additive. Cette fonctionnelle agrège les poids propres de toutes les structures intermédiaires de la forme mises en jeu au cours du processus d'assemblage par strates. Son analyse mathématique est esquissée et nous proposons un algorithme pour accélérer significativement les calculs coûteux entraînés par l'implémentation de ces idées. Une validation numérique ainsi qu'un exemple concret sont enfin présentés.

Contents

1. Introduction

The additive manufacturing technologies have demonstrated a unique potential in realizing structures with a high degree of complexity, thereby allowing to process almost directly the designs predicted by topology optimization algorithms [6]. These breakthroughs however come along with new challenges. One of them is to overcome the difficulty of building shapes showing large *overhangs*, i.e. regions hanging over void without sufficient support from the lower structure. Hitherto, ad hoc criteria, based on a minimum angle between the structural boundary and the horizontal directions, have been used to tackle this issue [7, 8, 9].

This brief note prefigures a longer article [2], devoted to several geometric or mechanical models for constraints related to additive manufacturing, and here we only focus on one of them. For simplicity, we assume that the components of one single layer of material are built simultaneously during the manufacturing

process; we then introduce a functional which appraises the constructibility of the shape at each stage of its assembly; in particular, overhang constraints are naturally addressed by this formulation. To achieve our purpose, in the setting of the optimization problem, we distinguish the mechanical situation where the (completed) shape Ω is utilized, on which the optimization criterion is based, and that where Ω (and all its intermediate structures) is under construction, which guides the definition of our constraint functional.

This note is organized as follows. In Section 2, we introduce our shape optimization problem. In Section 3, we describe the mechanical context in which Ω is constructed, and we formulate our manufacturing constraint accordingly. The resulting function of the domain and its shape derivative are quite costly to evaluate in practice, and we present in Section 4 an algorithm taking advantage of their intrinsic structure, which allows to accelerate significantly these calculations. Eventually, a numerical example is provided in Section 5.

2. Presentation of the shape optimization problem

A shape is a bounded, regular domain $\Omega \subset \mathbb{R}^d$, $d = 2, 3$, filled with a linear elastic material with Hooke's law A. In the context of its final utilization, Ω is clamped on a subset $\Gamma_D \subset \partial\Omega$, and it is submitted to surface loads $f \in L^2(\Gamma_N)^d$ applied on a region Γ_N of $\partial\Omega$ disjoint from Γ_D. The elastic displacement u_Ω^m is the unique solution in $H^1_{\Gamma_D}(\Omega)^d := \left\{u \in H^1(\Omega)^d,\ u = 0 \text{ on } \Gamma_D\right\}$ to the *mechanical* system:

$$\begin{cases} -\mathrm{div}(Ae(u_\Omega^m)) = 0 & \text{in } \Omega, \\ u_\Omega^m = 0 & \text{on } \Gamma_D, \\ Ae(u_\Omega^m)n = 0 & \text{on } \Gamma, \\ Ae(u_\Omega^m)n = f & \text{on } \Gamma_N. \end{cases} \tag{2.1}$$

For simplicity, the objective $J(\Omega)$ driving the optimization problem is the *compliance*:

$$J(\Omega) = \int_\Omega Ae(u_\Omega^m) : e(u_\Omega^m)\, dx = \int_{\Gamma_N} f \cdot u_\Omega^m\, ds. \tag{2.2}$$

Our optimization problem then reads:

$$\min_{\Omega \in \mathcal{U}_{ad}} J(\Omega), \text{ such that } P(\Omega) \leq \alpha, \tag{2.3}$$

in which $\mathcal{U}_{ad}$ is a set of (smooth) admissible shapes Ω, whose boundaries enclose the non optimizable regions Γ_D, Γ_N and Γ_0 (see Section 3 below for the definition of the latter), $P(\Omega)$ is a constraint functional, whose definition and properties are discussed in the next sections, and α is a tolerance threshold.

Most popular optimization algorithms for the numerical resolution of (2.3) rely on the derivatives of $J(\Omega)$ and $P(\Omega)$ with respect to the domain; these are understood in the framework of Hadamard's method (see e.g. [1, 10, 12, 13]): a generic function $F(\Omega)$ of the domain is *shape differentiable* if the underlying mapping $\theta \mapsto F((\mathrm{Id} + \theta)(\Omega))$, from $W^{1,\infty}(\mathbb{R}^d, \mathbb{R}^d)$ into $\mathbb{R}$, is Fréchet differentiable at $\theta = 0$; the corresponding derivative is denoted by $F'(\Omega)(\theta)$. Often, the deformations θ featured in this definition are restrained to a subset $\Theta_{ad} \subset W^{1,\infty}(\mathbb{R}^d, \mathbb{R}^d)$ of admissible displacements, so that deformations $(\mathrm{Id} + \theta)(\Omega)$ of admissible shapes Ω stay admissible.

As an example, if g is smooth, it is well-known (see e.g. [4]) that the shape derivative of (2.2) reads:

$$\forall \theta \in \Theta_{ad},\ \ J'(\Omega)(\theta) = -\int_\Gamma Ae(u_\Omega^m) : e(u_\Omega^m)\, \theta \cdot n\, ds.$$

3. Description and analysis of the mechanical constraint

3.1. Formulation of the constraint functional $P(\Omega)$.

The constraint $P(\Omega)$ relies on the mechanical situation of Ω in the course of the manufacturing process: Ω is enclosed in a box $D = S \times (0, H)$, $S \subset \mathbb{R}^{d-1}$, representing the build chamber with a vertical built direction e_d. For $h \in (0, H)$, $\Omega_h := \Omega \cap \left\{x = (x_1, ..., x_d) \in \mathbb{R}^d,\ 0 < x_d < h\right\}$ is the intermediate shape describing the

stage where Ω is assembled up to height h. The boundary $\partial\Omega_h$ is decomposed in a different fashion from that of Section 2:

$$\partial\Omega_h = \Gamma_0 \cup \Gamma_h^l \cup \Gamma_h^u, \text{ where } \begin{array}{l} \bullet\ \Gamma_0 = \{x \in \partial\Omega_h,\ \ x_d = 0\} \text{ is the contact region between } \Omega \text{ and the build table,} \\ \bullet\ \Gamma_h^u = \{x \in \partial\Omega_h,\ \ x_d = h\} \text{ is the upper side of the intermediate structure,} \\ \bullet\ \Gamma_h^l = \partial\Omega_h \setminus \overline{\Gamma_0 \cup \Gamma_h^u} \text{ is the lateral surface.} \end{array}$$

Eventually, we define $\ell_h := \{x \in \partial\Omega,\ \ x_d = h\}$, the part of the boundary $\partial\Omega$ that lies at height h.

Each intermediate shape Ω_h is clamped on Γ_0, and is only subjected to gravity effects, accounted for by a body force $g \in L^2(\mathbb{R}^d)^d$. Its elastic displacement $u^c_{\Omega_h} \in H^1_{\Gamma_D^c}(\Omega_h)^d$ satisfies:

$$\left\{ \begin{array}{cl} -\mathrm{div}(Ae(u^c_{\Omega_h})) = g & \text{in } \Omega_h, \\ u^c_{\Omega_h} = 0 & \text{on } \Gamma_0, \\ Ae(u^c_{\Omega_h})n = 0 & \text{on } \Gamma_h^l \cup \Gamma_h^u, \end{array} \right. \tag{3.1}$$

The compliance c_{Ω_h} of Ω_h then reads:

$$c_{\Omega_h} = \int_{\Omega_h} Ae(u^c_{\Omega_h}) : e(u^c_{\Omega_h})\, dx = \int_{\Omega_h} g \cdot u^c_{\Omega_h}\, dx. \tag{3.2}$$

Our constraint $P(\Omega)$ of the *total* structure Ω aggregates the compliances of all the intermediate shapes:

$$P(\Omega) = \int_0^H j(c_{\Omega_h})\, dh, \text{ where } j : \mathbb{R} \to \mathbb{R} \text{ is smooth.} \tag{3.3}$$

Remark 1. It is only incidental that similar mechanical models (that is, linear elasticity systems) are used for describing the mechanical and manufacturing stages. One could very well imagine modelling cooling effects with a constraint involving the temperature of the intermediate shapes Ω_h via the heat equation [3].

3.2. **Shape derivative of $P(\Omega)$.**

Let us introduce some additional notations: when $x \in \partial\Omega$, $n_S(x) := n(x) - (n(x) \cdot e_d)e_d$ denotes the orthogonal projection of the normal vector to Ω on the 'horizontal space', spanned by $e_1, ..., e_{d-1}$, and we consider a fixed shape $\Omega \in \mathcal{U}_{ad}$ satisfying the following geometric condition:

$$n_S(x) \text{ vanishes at most at a finite number of points } x \in \Gamma_H^l. \tag{3.4}$$

In other words, the total lateral boundary Γ_H^l does not contain any 'horizontal flat region'.

Under this assumption, the relevant set of perturbations for Ω is the Banach space

$$X = \left\{ \theta = |n_S|^2 \tilde{\theta},\ \ \tilde{\theta} \in \Theta_{ad} \right\}, \text{ equipped with the norm } ||\theta||_X = ||\frac{1}{|n_S|^2}\theta||_{\Theta_{ad}}. \tag{3.5}$$

In particular, vector fields $\theta \in X$ vanish at the points of $\partial\Omega$ where the normal vector n is parallel to e_d. Notice the abuse of notations in (3.5) where $|n_S|^2$ stands for any smooth extension of $|n_S|^2$ which does not vanish outside $\partial\Omega$. Our first result is (see [2] for the proof):

Theorem 1. *The functional $P(\Omega)$ defined by (3.3) is shape differentiable at any admissible shape $\Omega \in \mathcal{U}_{ad}$ satisfying (3.4), in the sense that the mapping $\theta \mapsto P(\Omega_\theta)$, from X into $\mathbb{R}$ is differentiable. Its derivative is:*

$$\forall \theta \in X,\ \ P'(\Omega)(\theta) = \int_{\Gamma_H^l} \mathcal{D}_\Omega\, \theta \cdot n\, ds, \tag{3.6}$$

where the integrand factor $\mathcal{D}_\Omega$ is defined by:

$$\mathcal{D}_\Omega(x) = \int_{x_d}^H j'(c_{\Omega_h}) \left(2g \cdot u^c_{\Omega_h} - Ae(u^c_{\Omega_h}) : e(u^c_{\Omega_h}) \right)(x)\, dh, \text{ for a.e. } x \in \Gamma_H^l. \tag{3.7}$$

Note that, due to the built direction constraint, the shape variations in Theorem 1 are not the standard ones.

4. Practical calculation of the mechanical constraint and its derivative

The numerical evaluation of $P(\Omega)$ and $P'(\Omega)(\theta)$, or equivalently $\mathcal{D}_\Omega$, rely on a discretization of the height interval $(0,H)$ with a sequence $0=h_0<h_1<...<h_N=H$. The intuitive, '0^{th}-order' method to calculate approximations P_N^0 and $\mathcal{D}_N^0$ of $P(\Omega)$ and $\mathcal{D}_\Omega$ consists in replacing c_{Ω_h} and $u^c_{\Omega_h}$ by their respective values at $h=h_{i+1}$ on each interval $I_i:=(h_i,h_{i+1})$. Doing so is costly since the subdivision $\{h_i\}_{i=0,...,N}$ of $(0,H)$ has to be fine enough to guarantee the accuracy of this approximation process; this brings about many numerical resolutions of the elasticity system (3.1) for the $u^c_{\Omega_{h_i}}$. An alternative idea relies on a higher-order reconstruction of the mappings $h\mapsto c_{\Omega_h}$ and $h\mapsto u^c_{\Omega_h}$ on each interval I_i.

4.1. Derivatives of the mappings $h\mapsto c_{\Omega_h}$ and $h\mapsto u^c_{\Omega_h}$.

Throughout this section, we consider a fixed shape $\Omega\in\mathcal{U}_{ad}$, and a value $h\in(0,H)$ satisfying:

$$\text{For any } x\in\ell_h,\ \text{the normal vector } n(x) \text{ is not parallel to } e_d. \tag{4.1}$$

Our first result concerns the derivative of $h\mapsto c_{\Omega_h}$; see [2] for proof.

Proposition 2. *In the above context, the mapping $h\mapsto c_{\Omega_h}$ is differentiable at h and:*

$$\frac{d}{dh}(c_{\Omega_h})\Big|_h=\int_{\Gamma_h^u}(2g\cdot u^c_{\Omega_h}-Ae(u^c_{\Omega_h}):e(u^c_{\Omega_h}))\,ds.$$

Let us now get interested in the differentiation of the mapping $h\mapsto u^c_{\Omega_h}$, in a suitable sense. In this direction, we prove in [2] that (see also [1, 11] for related notions):

- There exists $t_0>0$ and a mapping $(-t_0,t_0)\ni t\mapsto\phi_t$ satisfying the properties:

$$\begin{aligned}&\text{(i) For } t\in(-t_0,t_0),\ \phi_t \text{ is a diffeomorphism of } \mathbb{R}^d, \text{ mapping } \Omega_h \text{ onto } \Omega_{h-t} \text{ such that } \phi_t(\Gamma_0)=\Gamma_0,\\ &\text{(ii) The mapping } (-t_0,t_0)\ni t\mapsto(\phi_t-\mathrm{Id})\in W^{1,\infty}(\mathbb{R}^d,\mathbb{R}^d) \text{ is of class } \mathcal{C}^1,\\ &\text{(iii) Introducing } V(x):=\tfrac{d\phi_t(x)}{dt}|_{t=0}\in W^{1,\infty}(\mathbb{R}^d,\mathbb{R}^d), \text{ one has, for } x\in\Gamma_h^u,\ V(x)\cdot e_d=-1, \text{ and for}\\ &\quad x\in\Gamma_h^l,\ V(x)\cdot n(x)=0.\end{aligned} \tag{4.2}$$

- The mapping $t\mapsto u_{\Omega^c_{h-t}}\circ\phi_t$ is differentiable from $(-t_0,t_0)$ into $H^1_{\Gamma_0}(\Omega_h)^d$. Its derivative at $t=0$ is called the *Lagrangian derivative* Y_{Ω_h} of $h\mapsto u_{\Omega^c_h}$.
- The quantity $U_{\Omega_h}:=Y_{\Omega_h}-\nabla u_{\Omega^c_h}V$, which we identify as the *Eulerian derivative* of $h\mapsto u^c_{\Omega_h}$ is the natural candidate for defining its 'derivative'. U_{Ω_h} is the solution in $H^1_{\Gamma_0}(\Omega_h)^d$ to the system:

$$\begin{cases}-\mathrm{div}(Ae(U_{\Omega_h}))=0 & \text{in } \Omega_h,\\ U_{\Omega_h}=0 & \text{on } \Gamma_0,\\ Ae(U_{\Omega_h})n=0 & \text{on } \Gamma_h^l,\\ Ae(U_{\Omega_h})n=\frac{\partial}{\partial n}\left((Ae(u_{\Omega^c_h})n\right) & \text{on } \Gamma_h^u.\end{cases} \tag{4.3}$$

  In particular, U_{Ω_h} is independent of the mapping ϕ_t used in its definition as long as it fulfills (4.2).

4.2. Practical algorithm.

The considerations of Section 4.1 suggest the following procedure for calculating first-order approximations P_N^1 and $\mathcal{D}_N^1$ of $P(\Omega)$ and $\mathcal{D}_\Omega$ respectively. This allows for an accurate and computationally efficient calculation of these quantities, using a coarser subdivision $\{h_i\}_{i=1,...,N}$ of $(0,H)$ than in the calculation of the 0^{th}-order approximate values P_N^0 and $\mathcal{D}_N^0$.

(1) For $i=0,...,N$ calculate the compliances $c_{\Omega_{h_i}}$ as (3.2) and the displacements $u^c_{\Omega_{h_i}}$ by solving (3.1).
(2) For $i=0,...,N$, calculate the derivative $\frac{d}{dh}(c_{\Omega_h})\big|_{h=h_i}$ of the compliance by using Proposition 2.
(3) For $i=1,...,N$, calculate the Eulerian derivative $U_{\Omega_{h_i}}$ at h_i by using (4.3).
(4) On each interval I_i, $i=0,...,N-1$, the compliance c_{Ω_h} is approximated by a cubic spline $\widetilde{c}_i(h)$ which is uniquely determined by the data:

$$\widetilde{c}_i(h_i)=c_{\Omega_{h_i}},\ \widetilde{c}_i(h_{i+1})=c_{\Omega_{h_{i+1}}},\ \widetilde{c}_i{}'(h_i)=\frac{d}{dh}(c_{\Omega_h})\Big|_{h_i},\ \text{and } \widetilde{c}_i{}'(h_{i+1})=\frac{d}{dh}(c_{\Omega_h})\Big|_{h_{i+1}}. \tag{4.4}$$

(5) For $i = 0, ..., N-1$ and $h \in I_i$, $u^c_{\Omega_h}$ is approximated by $\widetilde{u_h}$ defined by:

$$\widetilde{u_h}(x) = u^c_{\Omega_{h_{i+1}}}(x) + (h_{i+1} - h)\, U_{\Omega_{h_{i+1}}}(x), \text{ a.e. } x \in \Omega_h; \tag{4.5}$$

notice that the above relation does make sense for $x \in \Omega_h$ regardless of the height $h \in (h_i, h_{i+1})$ since $u^c_{\Omega_{h_{i+1}}}$ and $U_{\Omega_{h_{i+1}}}$ are well-defined on $\Omega_h \subset \Omega_{h_{i+1}}$.

5. Numerical illustrations

Let us consider the $2d$ MBB Beam test case: the considered shapes Ω are contained in a rectangular domain D of size 6×1. Due to symmetry, only half of D is meshed by 300×100 $\mathbb{Q}_1$ elements. In the context of their final utilization (described by the system (2.1)), the horizontal displacement of shapes is fixed on a small part of their lower-left side and both horizontal and vertical displacements are fixed on a small part of its lower-right side, and a unit vertical load $f = (0, -1)$ is applied at the middle of their upper side. When it comes to their construction (modelled by (3.1)), shapes are built vertically from bottom to top, so that Γ_0 coincides with the lower-side of D. The design Ω_0 on Figure 1 (top) is used for the numerical validation of our methods in Section 5.1 and is an initial guess for the shape optimization of Section 5.2.

5.1. **Validation of the approximations of Section 4.**

At first, we calculate the functional $P(\Omega)$ and its shape derivative $\mathcal{D}_\Omega$ in the particular case where $\Omega = \Omega_0$, by using a uniform subdivision of $(0, H)$ made of 100 layers and the 0^{th}-order approximation scheme, i.e. we evaluate P^0_{100} and $\mathcal{D}^0_{100}$, which serve as reference values for the comparisons in this section. We then calculate the 0^{th}- and 1^{st}-order approximations P^i_N and $\mathcal{D}^i_N$, $i = 0, 1$ associated to several subdivisions of $(0, H)$ made of N intervals with equal length. We are interested in the behavior of the relative errors:

$$\text{err}(P, N, i) = \frac{|P^i_N - P^0_{100}|}{P^0_{100}} \quad \text{and} \quad \text{err}(\mathcal{D}, N, i) = \frac{|\mathcal{D}^i_N - \mathcal{D}^0_{100}|}{\mathcal{D}^0_{100}}.$$

The results are displayed on Figure 1 (bottom): while the 1^{st}-order approximation method does not bring a lot of improvement when it comes to evaluating the constraint functional $P(\Omega)$, it allows for a substantial gain (i.e. a faster convergence with respect to the number N of subdivisions) in the evaluation of its derivative.

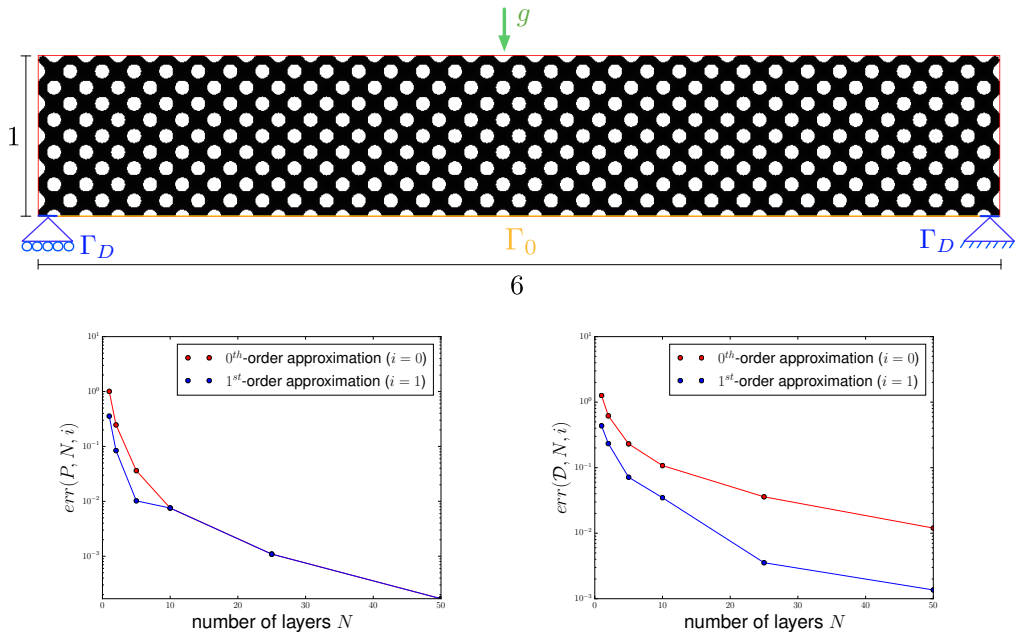

Figure 1. *(Top) Setting of the validation experiment and initial shape Ω_0; (bottom) relative errors of the 0^{th}- and 1^{st}-order approximations of $P(\Omega_0)$ and its derivative $\mathcal{D}_{\Omega_0}$.*

5.2. **A numerical example.**

We now turn to the shape optimization problem:

$$\min_{\Omega\in\mathcal{U}_{ad}} J(\Omega),\ \text{s.t. Vol}(\Omega)\leq 0.2\,\text{Vol}(D),\ \text{where } J(\Omega) \text{ is the compliance (2.2).} \tag{5.1}$$

We first solve (5.1), starting from the initial design Ω_0, by using an SLP-type algorithm in the spirit of that presented in [5], and the level set method on a fixed Cartesian mesh when it comes to tracking the deformation of shapes [4]. The optimized design Ω^* is shown in Figure 2; in particular, several overhanging parts appear in Ω^*.

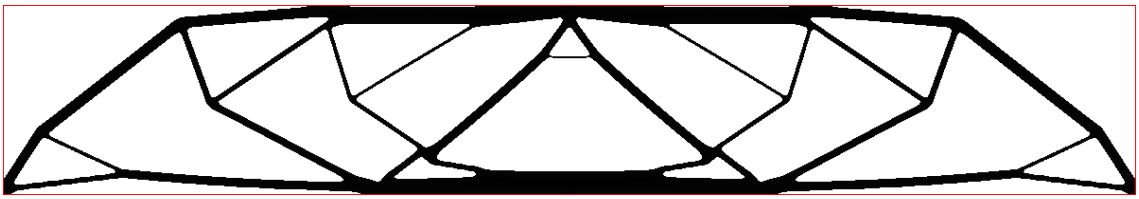

FIGURE 2. *Optimized design Ω^* for the shape optimization problem (5.1).*

We now add our mechanical constraint $P(\Omega)$ to this problem, and now solve:

$$\min_{\Omega\in\mathcal{U}_{ad}} J(\Omega)\ \text{s.t.}\ \left\{\begin{array}{c}\text{Vol}(\Omega)\leq 0.2\,\text{Vol}(D),\\ P(\Omega)\leq 0.5\,P(\Omega^*).\end{array}\right. \tag{5.2}$$

The resulting optimized shapes, obtained by using 0^{th}- and 1^{st}-order approximations of $P(\Omega)$ and $\mathcal{D}_\Omega$ with different (uniform) subdivisions of $(0,H)$ are represented on Figure 3. The computational effort is significantly different: about 237 h. are needed when the 0^{th}-order approximation process is used with $N=100$ layers, whereas the total calculation takes 'only' 82 h. when using 1^{st}-order approximations and $N=25$ layers. The values of the corresponding quantities of interest are collected in Table 1. Notice that several overhangs placed at the lower part of the optimal shape Ω^* without manufacturing constraint have vanished. It is also remarkable that the value of the objective function is lower for the constrained problem, meaning that the constraint has the (surprising) effect of driving the algorithm in a lower local minimum (this may be due to the larger number of iterations in the latter case).

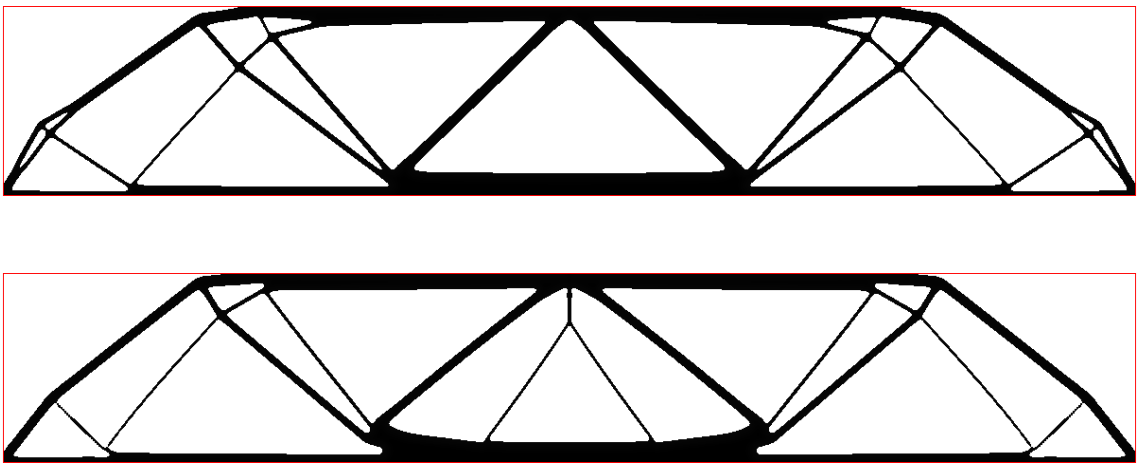

FIGURE 3. *Optimized shapes for (5.2) using the respective approximations for $P(\Omega)$ and $\mathcal{D}_\Omega$: (up) P^0_{100} and $\mathcal{D}^0_{100}$; (down) P^1_{25} and $\mathcal{D}^1_{25}$.*

Shape Ω	$J(\Omega)$	Vol(Ω)	$P(\Omega)$	Iterations	Evaluations
Figure 2	104.165	0.600	0.730	25	38
Figure 3 (up)	98.484	0.599	0.343	127	143
Figure 3 (down)	99.313	0.600	0.343	187	206

TABLE 1. *Values of the shape functionals and iteration numbers in the example of Section 5.2*

Acknowledgements. We thank Rafael Estevez for frutiful discussions during the course of this research.

REFERENCES

[1] G. ALLAIRE, *Conception optimale de structures*, vol. 58 of Mathématiques & Applications, Springer-Verlag, Berlin, (2007).
[2] G. ALLAIRE, C. DAPOGNY, A. FAURE, AND G. MICHAILIDIS, *Structural optimization under overhang constraints imposed by additive manufacturing technologies*, (in preparation).
[3] G. ALLAIRE, L. JAKABCIN, *Taking into account thermal residual stresses in topology optimization of structures built by additive manufacturing*, (in preparation).
[4] G. ALLAIRE AND F. JOUVE AND A.M. TOADER, *Structural optimization using shape sensitivity analysis and a level-set method*, J. Comput. Phys., 194 (2004) pp. 363–393.
[5] P. DUNNING AND H. KIM, *Introducing the sequential linear programming level-set method for topology optimization*, Structural and Multidisciplinary Optimization, 51 (2015), pp. 631–643.
[6] I. GIBSON, D.W. ROSEN AND B. STUCKER, *Additive manufacturing technology: rapid prototyping to direct digital manufacturing*, Springer Science Business Media, Inc, (2010).
[7] A.T. GAYNOR AND J.K. GUEST, *Topology optimization considering overhang constraints: Eliminating sacrificial support material in additive manufacturing through design*, Struct. Multidisc. Optim., (2016), doi:10.1007/s00158-016-1551-x.
[8] M. LANGELAAR, *Topology optimization of 3D self-supporting structures for additive manufacturing*, Additive Manufacturing, 12, (2016), pp. 60–70.
[9] A. M. MIRZENDEHDEL AND K. SURESH, *Support structure constrained topology optimization for additive manufacturing*, Computer-Aided Design, (2016), http://dx.doi.org/10.1016/j.cad.2016.08.006.
[10] F. MURAT AND J. SIMON, *Sur le contrôle par un domaine géométrique*, Technical Report RR-76015, Laboratoire d'Analyse Numérique (1976).
[11] A. NOVOTNY AND J. SOKOLOWSKI, *Topological derivatives in shape optimization*, Springer, Heidelberg (2012).
[12] O. PIRONNEAU, *Optimal shape design for elliptic systems*, Springer-Verlag, New York (1984).
[13] J. SOKOŁOWSKI, J.-P. ZOLESIO, *Introduction to shape optimization: shape sensitivity analysis*, Springer Series in Computational Mathematics, Vol. 10, Springer, Berlin (1992).